

## The Ultra Weak Variational Formulation Using Bessel Basis Functions

Teemu Luostari<sup>1,\*</sup>, Tomi Huttunen<sup>1</sup> and Peter Monk<sup>2</sup>

<sup>1</sup> Department of Applied Physics, University of Eastern Finland, P.O. Box 1627, FI-70211 Kuopio, Finland.

<sup>2</sup> Department of Mathematical Sciences, University of Delaware, Newark, DE 19716, USA.

Received 12 December 2009; Accepted (in revised version) 4 January 2011

Available online 24 October 2011

---

**Abstract.** We investigate the ultra weak variational formulation (UWVF) of the 2-D Helmholtz equation using a new choice of basis functions. Traditionally the UWVF basis functions are chosen to be plane waves. Here, we instead use first kind Bessel functions. We compare the performance of the two bases. Moreover, we show that it is possible to use coupled plane wave and Bessel bases in the same mesh. As test cases we shall consider propagating plane and evanescent waves in a rectangular domain and a singular 2-D Helmholtz problem in an  $L$ -shaped domain.

**PACS:** 02.60.Cb, 02.60.Lj, 02.70.Dh, 43.20.-f

**Key words:** The ultra weak variational formulation, Helmholtz problem, plane wave basis, Bessel basis, non-polynomial basis.

---

### 1 Introduction

Interest in methods which use non-polynomial basis functions has increased recently because of their potential computational efficiency, especially, for higher frequency problems. Nevertheless, the numerical approximation of wave propagation problems still remains challenging and time consuming. One of these non-polynomial basis functions methods, herein studied, is called the ultra weak variational formulation (UWVF). The UWVF was first introduced and analyzed by Cessenat and Després [6–8] for the Helmholtz equation and Maxwell equations. To date the UWVF has been applied in many physical problems, for example, audio acoustics [21], ultrasound acoustics [17], electromagnetics [18], optoelectronics [22] and elasticity [19].

---

\*Corresponding author. *Email addresses:* teemu.luostari@uef.fi (T. Luostari), tomi.huttunen@uef.fi (T. Huttunen), monk@math.udel.edu (P. Monk)

The UWVF is a volume based method and uses triangular or tetrahedral meshes similar to those used in the finite element method (FEM). However, in the UWVF, solutions are computed on element edges in the 2-D case (and on element faces in the 3-D case). When simulating at high frequencies, the UWVF is more efficient than traditional FEM, see, for example, [8].

The original UWVF uses plane waves as a basis functions in part because integrals encountered in the method can be computed efficiently in closed form. Other non-polynomial basis methods include the discontinuous enrichment method (DEM) [9], partition of unity finite element method (PUFEM) [23], least squares method (LSM) [24] and discontinuous Galerkin method (DGM) [10]. In fact, it has been recently shown (see [11, 18]) that the UWVF is a special form of an upwind DGM. Some of these methods (PUFEM, LSM, UWVF and DGM) have also been compared to each other for 2-D Helmholtz problems.

Namely, the UWVF and PUFEM were compared to each other in [16] where the authors showed that the UWVF worked better at high frequencies and PUFEM at low frequencies. It has also been shown in [13] that at high frequencies the UWVF and DGM provide better accuracy than LSM while at low frequencies all three methods have similar errors. The use of Bessel basis functions has been studied in the DGM applying them to ultrasound and electromagnetic problems [2], and in the LSM [24].

In the UWVF, accuracy can be improved by refining the grid and/or using more basis functions on an element. However, if the elements are small compared to the wavelength, or too many basis functions are used, or when simulating at low frequencies, ill-conditioning may occur. One possible technique for improving the UWVF at low frequencies is to use a hybridized mixed FEM introduced in reference [25]. However, motivated by the work of Gittelsohn, Hiptmair and Perugia [14] and Barnett and Betcke [3], Bessel basis functions are considered in this paper. The goal is to improve the UWVF for problems with small elements or singularities. Unfortunately, for the Bessel basis, the UWVF-integrals must be computed using quadratures. On the other hand, Barnett and Betcke [3] reported interesting results for problems with singularities using only Bessel basis functions. Our intention is to use plane wave basis and Bessel basis functions in the UWVF.

We shall study 2-D Helmholtz problems. One of our model problems will be a singular 2-D Helmholtz problem on an  $L$ -shaped domain that was also a model problem in [12, 16]. In addition, we shall study propagating plane and evanescent waves in a rectangular domain.

This paper is organized as follows. In Section 2 the Helmholtz problem and UWVF are introduced. In Section 3 the different choices of basis functions are given. Section 4 is devoted to numerical simulations and is divided in two parts: the first problem studies a propagating plane wave and evanescent wave in a rectangular domain and second studies a singular 2-D Helmholtz problem. Finally, we draw conclusions in Section 5.

## 2 The ultra weak variational formulation

Let  $\Omega$  be a bounded polygonal domain in  $\mathbb{R}^2$  with the boundary  $\Gamma$  and unit outward normal  $\mathbf{n}$ . We consider the homogeneous Helmholtz problem: find  $u$  such that

$$\Delta u + \kappa^2 u = 0, \quad \text{in } \Omega, \quad (2.1a)$$

$$\frac{\partial u}{\partial \mathbf{n}} - i\sigma u = Q \left( -\frac{\partial u}{\partial \mathbf{n}} - i\sigma u \right) + g, \quad \text{on } \Gamma, \quad (2.1b)$$

where  $\kappa \neq 0$  is the wavenumber,  $\sigma$  is the coupling parameter (real and positive, usually  $\sigma = \Re\{\kappa\}$ ),  $Q \in \mathbb{C}$ ,  $|Q| \leq 1$ , defines the type of the boundary condition and  $g$  is the source term on the boundary. From Eq. (2.1b) the following boundary conditions can be derived: Neumann boundary condition ( $Q=1$ ), Dirichlet boundary condition ( $Q=-1$ ) and mixed or the Robin boundary condition ( $Q \neq 1, -1$ ). In addition, with the choice  $Q=0$ ,  $g=0$  and  $\sigma = \kappa$ . Eq. (2.1b) corresponds to the lowest order Engquist Majda absorbing boundary condition.

Following the original work of Cessenat and Després [6, 8] the ultra weak variational formulation can be derived using a Trefftz-type approach [12] or a discontinuous Galerkin (DG) approach [4, 18]. The DG approach outlined herein follows the techniques from references [1, 4].

Let us introduce a field  $v$  such that  $i\kappa v = -\nabla u$ . Then we can write the Helmholtz problem (2.1a)-(2.1b) as a first order system

$$-i\kappa v = \nabla u, \quad \text{in } \Omega, \quad (2.2a)$$

$$-i\kappa u = \nabla \cdot v, \quad \text{in } \Omega, \quad (2.2b)$$

$$-i\kappa v \cdot \mathbf{n} - i\sigma u = Q(i\kappa v \cdot \mathbf{n} - i\sigma u) + g, \quad \text{on } \Gamma. \quad (2.2c)$$

We partition the domain  $\Omega$  into non-overlapping elements  $\Omega_k$  such that  $\Omega = \bigcup_{k=1}^N \Omega_k$  (see Fig. 1 for some notation related to the mesh).

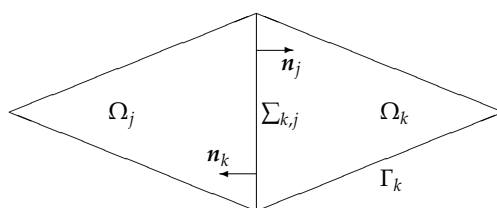


Figure 1: The exterior boundary of an element  $\Omega_k$  is denoted by  $\Gamma_k$  and the outward unit normal by  $\mathbf{n}_k$ . The interface between elements  $\Omega_k$  and  $\Omega_j$  is denoted as  $\Sigma_{k,j}$ .

Let  $u_k = u|_{\Omega_k}$  and  $v_k = v|_{\Omega_k}$ . Multiplying Eqs. (2.2a) and (2.2b) by the complex conjugate of a smooth test vector  $\tau_k$  and a scalar  $\phi_k$ , respectively, and integrating over an element

$\Omega_k$  we have

$$\int_{\Omega_k} (-i\kappa \mathbf{v}_k \cdot \bar{\boldsymbol{\tau}}_k + u_k \nabla \cdot \bar{\boldsymbol{\tau}}_k) dV = \int_{\partial\Omega_k} u \mathbf{n}_k \cdot \bar{\boldsymbol{\tau}}_k dA, \quad (2.3a)$$

$$\int_{\Omega_k} (-i\kappa u_k \cdot \bar{\boldsymbol{\phi}}_k + \mathbf{v}_k \cdot \nabla \bar{\boldsymbol{\phi}}_k) dV = \int_{\partial\Omega_k} \mathbf{v} \cdot \mathbf{n}_k \bar{\boldsymbol{\phi}}_k dA, \quad (2.3b)$$

where  $\mathbf{n}_k$  is the outward normal unit vector to the element  $\Omega_k$ .

Adding Eqs. (2.3a) and (2.3b) and replacing in the right hand side  $u$  by  $\hat{u}$  and  $\mathbf{v}$  by  $\hat{\mathbf{v}}$  (to be specified shortly), one obtains

$$\int_{\Omega_k} (\mathbf{v}_k \cdot \overline{(i\kappa \boldsymbol{\tau}_k + \nabla \boldsymbol{\phi}_k)} + u_k \overline{(i\kappa \boldsymbol{\phi}_k + \nabla \cdot \boldsymbol{\tau}_k)}) dV = \int_{\partial\Omega_k} (\hat{u} \mathbf{n}_k \cdot \bar{\boldsymbol{\tau}}_k + \hat{\mathbf{v}} \cdot \mathbf{n}_k \bar{\boldsymbol{\phi}}_k) dA.$$

Choosing  $\boldsymbol{\tau}$  and  $\boldsymbol{\phi}$  to be smooth solutions of the adjoint Helmholtz problem

$$\overline{(i\kappa \boldsymbol{\tau}_k + \nabla \boldsymbol{\phi}_k)} = 0 \quad \text{and} \quad \overline{(i\kappa \boldsymbol{\phi}_k + \nabla \cdot \boldsymbol{\tau}_k)} = 0, \quad \text{in } \Omega_k, \quad (2.4)$$

we obtain

$$\int_{\partial\Omega_k} (\hat{u} \mathbf{n}_k \cdot \bar{\boldsymbol{\tau}}_k + \hat{\mathbf{v}} \cdot \mathbf{n}_k \bar{\boldsymbol{\phi}}_k) dA = 0. \quad (2.5)$$

We use Eq. (2.5) on each element by giving definitions for the fluxes  $\hat{u}$  and  $\hat{\mathbf{v}}$ . Using a DG approach we introduce standard notation for averages and jumps as follows

$$\{\{u\}\} = \frac{u_k + u_j}{2}, \quad \{\{v\}\} = \frac{v_k + v_j}{2}, \quad (2.6a)$$

$$[[u]] = u_k \mathbf{n}_k + u_j \mathbf{n}_j, \quad [[v]] = v_k \cdot \mathbf{n}_k + v_j \cdot \mathbf{n}_j. \quad (2.6b)$$

On interior faces we define fluxes, using a similar strategy to reference [15], by

$$\hat{u} = \{\{u\}\} - \frac{\kappa}{2\sigma} [[v]] \quad \text{and} \quad \hat{\mathbf{v}} = \{\{v\}\} - \frac{\sigma}{2\kappa} [[u]]. \quad (2.7)$$

Multiplying Eq. (2.5) by  $\kappa$  and using the fluxes (2.7), the definitions of averages and jumps (2.6a)-(2.6b), Eq. (2.5) can be rearranged, for an interior edge, to obtain

$$\begin{aligned} & \int_{\Sigma_{k,j}} \kappa (\hat{u} \mathbf{n}_k \cdot \bar{\boldsymbol{\tau}}_k + \hat{\mathbf{v}} \cdot \mathbf{n}_k \bar{\boldsymbol{\phi}}_k) dA \\ &= - \int_{\Sigma_{k,j}} \frac{1}{2\sigma} [(-i\sigma u_k + i\kappa \mathbf{v}_k \cdot \mathbf{n}_k) \overline{(-i\sigma \boldsymbol{\phi}_k + i\kappa \mathbf{n}_k \cdot \boldsymbol{\tau}_k)}] dA \\ & \quad + \int_{\Sigma_{k,j}} \frac{1}{2\sigma} [(-i\sigma u_j + i\kappa \mathbf{v}_j \cdot \mathbf{n}_j) \overline{(-i\sigma \boldsymbol{\phi}_k - i\kappa \boldsymbol{\tau}_k \cdot \mathbf{n}_k)}] dA \\ &= - \int_{\Sigma_{k,j}} \frac{1}{2\sigma} \mathcal{X}_k \bar{\mathcal{Y}}_k dA + \int_{\Sigma_{k,j}} \frac{1}{2\sigma} \mathcal{X}_j \overline{F_k(\mathcal{Y}_k)} dA, \end{aligned} \quad (2.8)$$

in which we have defined  $\mathcal{X}_k = (-i\sigma u_k + i\kappa v_k \cdot \mathbf{n}_k)$  (similarly  $\mathcal{X}_j$ ),  $\mathcal{Y}_k = (-i\sigma\phi_k + i\kappa \mathbf{n}_k \cdot \boldsymbol{\tau}_k)$  and  $F_k(\mathcal{Y}_k) = (-i\sigma\phi_k - i\kappa \boldsymbol{\tau}_k \cdot \mathbf{n}_k)$ .

On an exterior boundary edge  $\Gamma_k = \partial\Omega_k \cap \Gamma$ , we define fluxes  $\hat{v} = v$  and  $\hat{u} = u$ . Then, using the above definition of  $F_k(\mathcal{Y}_k)$ , we can write

$$\begin{aligned} & \int_{\Gamma_k} \kappa (u_k \mathbf{n}_k \cdot \bar{\boldsymbol{\tau}}_k + v_k \cdot \mathbf{n}_k \bar{\phi}_k) dA \\ &= - \int_{\Gamma_k} \frac{1}{2\sigma} (-i\sigma u_k + i\kappa v_k \cdot \mathbf{n}_k) \overline{(-i\sigma\phi_k + i\kappa \mathbf{n}_k \cdot \boldsymbol{\tau}_k)} dA \\ & \quad + \int_{\Gamma_k} \frac{1}{2\sigma} (-i\sigma u_k - i\kappa v_k \cdot \mathbf{n}_k) \overline{(-i\sigma\phi_k - i\kappa \mathbf{n}_k \cdot \boldsymbol{\tau}_k)} dA \\ &= - \int_{\Gamma_k} \frac{1}{2\sigma} \mathcal{X}_k \bar{\mathcal{Y}}_k dA + \int_{\Gamma_k} \frac{1}{2\sigma} F_k(\mathcal{X}_k) \overline{F_k(\mathcal{Y}_k)} dA. \end{aligned} \tag{2.9}$$

Adding Eqs. (2.8) and (2.9) and rearranging terms we can write Eq. (2.5) as

$$\int_{\partial\Omega_k} \frac{1}{\sigma} \mathcal{X}_k \bar{\mathcal{Y}}_k dA - \sum_{j=1, k \neq j}^N \int_{\Sigma_{k,j}} \frac{1}{\sigma} \mathcal{X}_j \overline{F_k(\mathcal{Y}_k)} dA = \int_{\Gamma_k} \frac{1}{\sigma} F_k(\mathcal{X}_k) \overline{F_k(\mathcal{Y}_k)} dA.$$

Taking into account the boundary condition from Eq. (2.2c) and summing over all elements we have the UWVF of finding  $\mathcal{X}_k \in L^2(\partial\Omega_k)$ ,  $k=1, \dots, N$ , such that

$$\begin{aligned} & \sum_{k=1}^N \int_{\partial\Omega_k} \frac{1}{\sigma} \mathcal{X}_k \bar{\mathcal{Y}}_k dA - \sum_{k=1}^N \sum_{j=1, k \neq j}^N \int_{\Sigma_{k,j}} \frac{1}{\sigma} \mathcal{X}_j \overline{F_k(\mathcal{Y}_k)} dA \\ & \quad - \sum_{k=1}^N \int_{\Gamma_k} \frac{Q}{\sigma} \mathcal{X}_k \overline{F_k(\mathcal{Y}_k)} dA = \sum_{k=1}^N \int_{\Gamma_k} \frac{1}{\sigma} g \overline{F_k(\mathcal{Y}_k)} dA \end{aligned} \tag{2.10}$$

for all  $\mathcal{Y}_k \in L^2(\partial\Omega_k)$ ,  $k=1, \dots, N$ .

The problem can be discretized by choosing basis function  $\{\varphi_{k,\ell}\}_{\ell=1}^{p_k}$  on  $\Omega_k$ ,  $1 \leq k \leq N$ , that satisfy Eq. (2.4). Then

$$\mathcal{X}_k^a = \sum_{\ell=1}^{p_k} \mathcal{X}_{k,\ell} \left( -\frac{\partial \varphi_{k,\ell}}{\partial \mathbf{n}_k} - i\sigma \varphi_{k,\ell} \right) \Big|_{\partial\Omega_k}, \tag{2.11}$$

where we have used Eqs. (2.2a) and (2.2b). Similarly for  $\mathcal{Y}_k$  we can write

$$\mathcal{Y}_k^a = \left( -\frac{\partial \varphi_{k,\ell}}{\partial \mathbf{n}_k} - i\sigma \varphi_{k,\ell} \right), \quad \text{for } 1 \leq \ell \leq p_k. \tag{2.12}$$

Using  $\mathcal{X}_k^a$  and  $\mathcal{Y}_k^a$  in Eq. (2.10) gives a non-singular matrix problem for the coefficients  $\{\mathcal{X}_{k,\ell}\}_{\ell=1, k=1}^{p_k, N}$  for any  $\kappa > 0$  [7]. In particular, using Eqs. (2.11) and (2.12), in (2.10) we can write the problem in a matrix form as  $(\mathbf{D} - \mathbf{C})\mathbf{X} = \mathbf{b}$  with unknown weights  $\mathbf{X} = (\mathcal{X}_{11}, \dots, \mathcal{X}_{1p_1}, \mathcal{X}_{21}, \dots)^T$ . Matrices  $\mathbf{D}$  and  $\mathbf{C}$  are sparse block matrices and matrix  $\mathbf{D}$  is Hermitian block diagonal. In order to improve conditioning, we use the preconditioned form  $(\mathbf{I} - \mathbf{D}^{-1}\mathbf{C})\mathbf{X} = \mathbf{D}^{-1}\mathbf{b}$  (see [16, 20]).

### 3 Choice of basis functions

In the UWVF the basis functions are usually chosen to be plane waves because the integrals in (2.10) can be computed in closed form. The plane wave basis functions are defined by

$$\varphi_{k,\ell} = \exp(i\bar{\kappa}_k \mathbf{d}_{k,\ell} \cdot \mathbf{x}) \text{ in } \Omega_k \text{ and } 0 \text{ elsewhere,} \quad (3.1)$$

where the directions for the plane wave basis in element  $\Omega_k$  are given by

$$\mathbf{d}_{k,\ell} = \left( \cos\left(2\pi \frac{\ell-1}{p_k}\right), \sin\left(2\pi \frac{\ell-1}{p_k}\right) \right), \quad \ell = 1, \dots, p_k.$$

Considering the case when  $\kappa \rightarrow 0$ , we see that the plane wave basis behaves as

$$e^{i\bar{\kappa} \mathbf{d} \cdot \mathbf{x}} \approx 1 + i\bar{\kappa} \mathbf{x} \cdot \mathbf{d} + \mathcal{O}(|\bar{\kappa}|^2 |\mathbf{x}|^2) \rightarrow 1 \text{ as } \kappa \rightarrow 0.$$

Hence ill-conditioning is expected for small  $\kappa$  (or small  $h$ , or by other arguments for large  $p_k$ ). Trying to enhance the accuracy and avoid ill-conditioning we introduce a new basis using the Bessel functions of the first kind and order  $\ell$ . Motivated by the work of Gittelsohn, Hiptmair and Perugia [14] we use Bessel basis with a scaling term

$$\varphi_{k,\ell} = \frac{J_\ell(\bar{\kappa}_k |\mathbf{x}_k - \mathbf{x}_{0,k}|)}{J_\ell(\bar{\kappa}_k L_k)} e^{i\ell\theta} \text{ in } \Omega_k \text{ and } 0 \text{ elsewhere,} \quad (3.2)$$

where  $\ell$  is the order of Bessel function,  $\theta$  is the polar angle about  $\mathbf{x}_{0,k}$ , the centroid of the element  $\Omega_k$  and  $L_k$  is a scaling parameter. For the above Bessel basis with the scaling we have

$$\frac{J_\ell(\bar{\kappa} |\mathbf{x}_k - \mathbf{x}_{0,k}|)}{J_\ell(\bar{\kappa} L_k)} e^{i\ell\theta} \rightarrow \left(\frac{\bar{\kappa} r}{\bar{\kappa} L_k}\right)^\ell e^{i\ell\theta} = \left(\frac{r}{L_k}\right)^\ell e^{i\ell\theta} \text{ as } \kappa \rightarrow 0,$$

which represents harmonic polynomials suggesting better behavior at low frequencies or when the elements are small compared to the wavelength [14]. In addition, this suggests that  $L_k = h_k$  might be a useful choice. Another choice is a Bessel basis without scaling written as follows

$$\varphi_{k,\ell} = J_\ell(\bar{\kappa}_k |\mathbf{x}_k - \mathbf{x}_{0,k}|) e^{i\ell\theta} \text{ in } \Omega_k \text{ and } 0 \text{ elsewhere.} \quad (3.3)$$

In the case of a Bessel basis, the integrals in Eq. (2.10) must be computed using quadratures (here, Legendre-Gauss quadratures are used) and therefore it takes longer to compute the integrals than in the case of a plane wave basis. We have not attempted to optimize this aspect of the Bessel UWVF here and so do not report computer time.

The order  $\ell$  of the Bessel function basis in element  $\Omega_k$  is chosen to be

$$\ell = s - \frac{p_k - 1}{2} - 1,$$

where  $p_k$  is the number of basis functions and  $s = 1, \dots, p_k$ . We choose the order  $\ell$  to be an integer and therefore the number of basis functions  $p_k$  must be odd. We obtain Bessel function orders  $-\frac{p_k-1}{2}, \dots, \frac{p_k-1}{2}$ . Moreover, we require  $p_k \geq 3$ .

## 4 Numerical simulations

This section is divided in two parts: first we consider the propagating plane wave or evanescent wave problem in a rectangular domain and second we study singular 2-D Helmholtz problem. All simulations are coded using Matlab. The UWVF integrals (2.10) for Bessel bases are computed using 128 point Legendre-Gauss quadratures. This large number of points is used because we want to focus on basis functions and have a very accurate approximation of the integrals.

### 4.1 Propagating plane wave and evanescent wave in a rectangular domain

We will approximate the solution to the Helmholtz problem (2.1a)-(2.1b) on  $\Omega = [-1,1]^2$  with  $Q=0$  and  $g = \partial u_{ex} / \partial \mathbf{n} + i\sigma u_{ex}$ , where  $\sigma = \kappa$  and in the case of a plane wave source,  $u_{ex} = \exp(i\kappa \mathbf{d} \cdot \mathbf{x})$ . Here  $\mathbf{d} = (\cos(\pi/p), \sin(\pi/p))$  and  $p$  is the number of basis functions (the same number of directions is used in all elements in this experiment so  $p_k = p$  for all  $k$ ). In the case of an evanescent wave  $u_{ex} = \exp(i(\alpha_1(x+1) + \alpha_2 y))$ , where  $\alpha_1^2 + \alpha_2^2 = \kappa^2$ ,  $\alpha_1 = i\kappa\sqrt{\beta^2 - 1}$  and  $\alpha_2 = \beta\kappa$  with  $\beta > 1$ . In our simulations we make an arbitrary choice of  $\beta = 20$  when  $\kappa = 0.05$ .

The coarsest and densest uniform meshes are shown in Fig. 2.

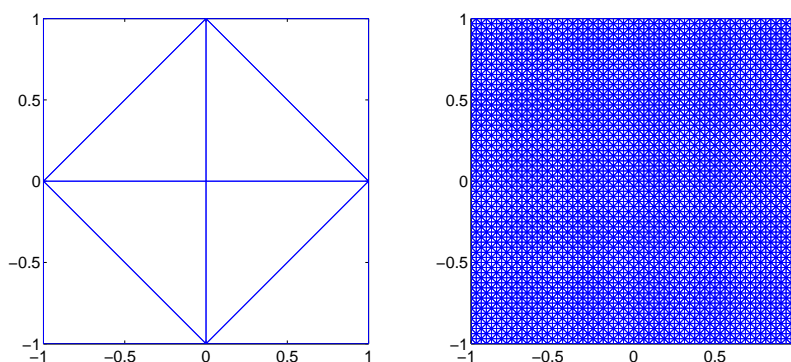


Figure 2: The computational domain is  $[-1,1] \times [-1,1]$ . The coarsest ( $h=1.0$ ) and densest ( $h=0.03125$ ) meshes for the rectangular domain. Meshes are derived from the coarse mesh by uniform subdivision.

As basis functions we consider the plane wave basis equation (3.1), Bessel basis with scaling equation (3.2) (term in denominator  $L_k = h$  for all  $k$ ) and Bessel basis without scaling equation (3.3). Results are shown in Fig. 3 when the wave number  $\kappa = 0.05$  on all elements, the number of basis functions  $p=5$  and the mesh size  $h$  varies. In this case the wavelength is  $\lambda = 2\pi/\kappa \approx 126$  so the domain is small compared to the wavelength and this is a low frequency problem.

On the right in Fig. 3 is shown the maximum condition number of the matrix  $\mathbf{D}$  versus the length of the shortest edge in the mesh and on the left, relative error (%) versus the

length of the edge. Relative errors are computed from

$$\text{error}(\%) = \frac{\|u_{ex} - u_{app}\|_{\ell^2}}{\|u_{ex}\|_{\ell^2}} \times 100\%, \quad (4.1)$$

where  $u_{ex}$  is the exact solution and  $u_{app}$  is the approximation using the UWVF. The relative errors are computed by interpolating to a uniform dense array of points.

Fig. 3 shows that Bessel basis with scaling has the lowest condition number and the plane wave basis and Bessel bases without scaling have almost the same condition numbers. However, the errors remain the same for both Bessel bases. For the plane wave propagation problem it can be seen that when the elements are small and the error level is small the effect of ill-conditioning increases the error for plane wave basis whereas errors for both Bessel bases remain decreasing. However, for the evanescent wave problem the ill-conditioning does not seem to affect the error levels. It is also noticeable that error levels for the evanescent wave problem are greater than error levels in the plane wave propagation problem even though the same number of basis functions is used, see also the case in Table 1 and Fig. 4 (see [26] for approximation theory relevant to this case). In addition, on the right in Fig. 3 we can see that condition number increase at the same rate as  $h \rightarrow 0$ , so scaling does not ultimately eliminate ill-conditioning.

In practice the UWVF is often used on a fixed mesh varying the number of basis functions  $p$ . Let us consider the evanescent wave problem varying  $p$  when  $\kappa = 0.05$  and the mesh size  $h = 0.25$ . Table 1 gives the error levels and in Fig. 4 is shown the 1-norm condition number of the matrix  $\mathbf{D}$  and the 1-norm condition number estimate of the problem, i.e.,  $\text{condest}(\mathbf{I} - \mathbf{D}^{-1}\mathbf{C})$ .

Table 1: Results for the evanescent wave problem using the plane wave basis, scaled Bessel basis and unscaled Bessel basis when  $\kappa = 0.05$  and  $h = 0.25$  on a square.

$p$	PW error (%)	scaled Bessel error (%)	unscaled Bessel error (%)
3	1.2667	1.2912	1.2914
5	0.2109	0.2179	0.2179
7	115.0009	0.0062	0.0062
9	8.3419e6	6.0748e-5	6.0746e-5

Results shown in Table 1 and Fig. 4 show that ill-conditioning may cause increasing of error for the plane wave basis whereas both Bessel bases act stably having converging error levels as a function of the number of basis functions. In addition, the scaling term in the Bessel basis has an affect damping the condition number of the matrix  $\mathbf{D}$  and the global condition number estimate of the problem. However, when  $p = 3$  the scaled Bessel basis has a greater condition number than plane wave basis and unscaled Bessel basis.

Results shown in Figs. 3 and 4 and in Table 1 show that ill-conditioning may hamper the accuracy for the plane wave basis if the error target is small. However, if the error level goal is, say  $\leq 1\%$ , it is more efficient to use plane wave basis functions in the UWVF. Nevertheless, the Bessel basis (scaled or unscaled) does enhance robustness.

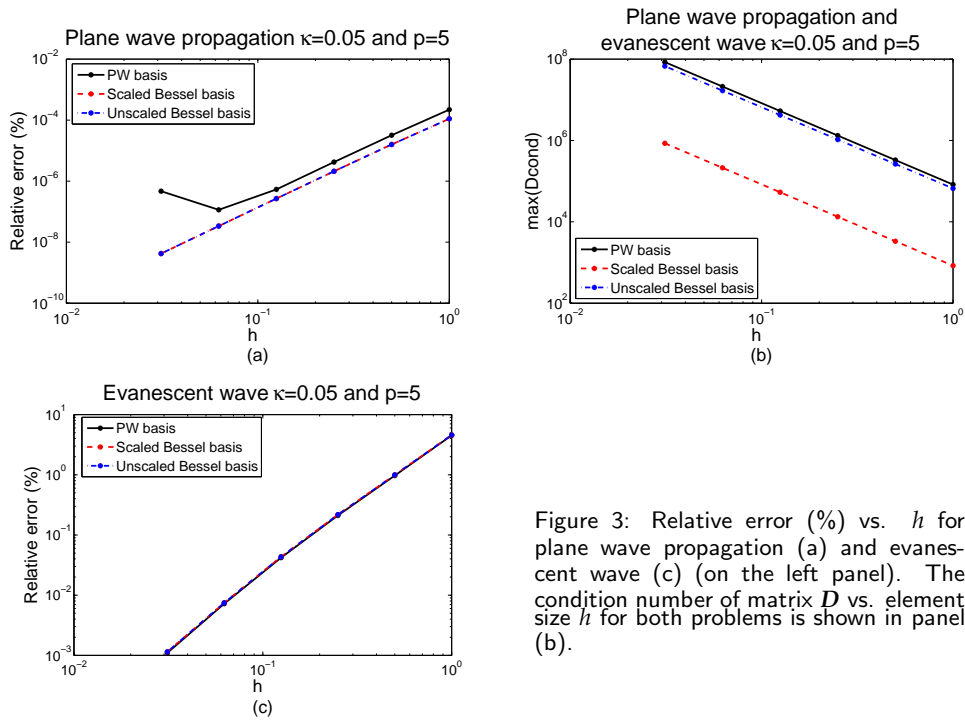


Figure 3: Relative error (%) vs.  $h$  for plane wave propagation (a) and evanescent wave (c) (on the left panel). The condition number of matrix  $D$  vs. element size  $h$  for both problems is shown in panel (b).

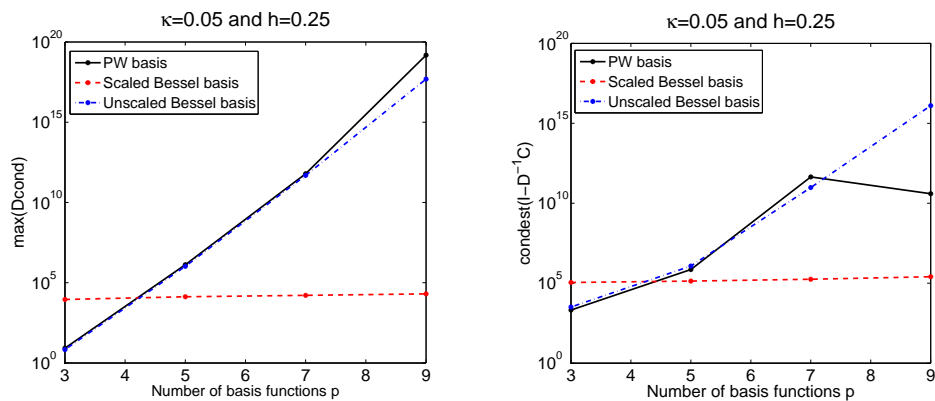


Figure 4: The 1-norm condition number of matrix  $D$  vs. the number of basis functions (on the left panel). The 1-norm condition number estimate for the problem,  $\text{condest}(\mathbf{I}-\mathbf{D}^{-1}\mathbf{C})$ , vs. the number of basis functions (on the right panel).

## 4.2 A singular Helmholtz problem

We now consider a singular solution to the Helmholtz problem in an  $L$ -shaped domain as a model problem, see Fig. 5. This test case is similar to the problem in references [12, 16]. The exterior boundary  $\Gamma$  is divided into two disjoint parts  $\Gamma_1$  and  $\Gamma_2$  and thus  $\Gamma = \Gamma_1 \cup \Gamma_2$ . The two edges meeting at the origin are denoted by  $\Gamma_1$  and the other edges belong to the

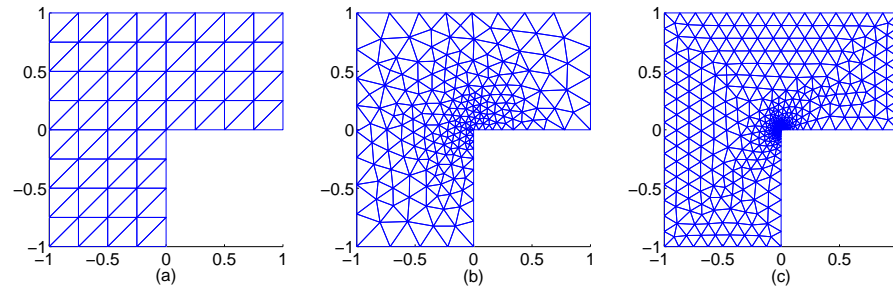


Figure 5: The  $L$ -shaped domain meshes used in simulations. The uniform mesh on the left consists of 65 vertices and 96 elements. The lightly refined non-uniform mesh on the center consists of 233 vertices and 422 elements. The densest non-uniform mesh on right consists of 704 vertices and 1304 elements.

boundary  $\Gamma_2$ . We want to approximate  $u$  such that

$$\begin{aligned} \Delta u + \kappa^2 u &= 0, & \text{in } \Omega, \\ u &= 0, & \text{on } \Gamma_1, \\ \frac{\partial u}{\partial \mathbf{n}} + i\sigma u &= \frac{\partial u_{ex}}{\partial \mathbf{n}} + i\sigma u_{ex}, & \text{on } \Gamma_2, \end{aligned}$$

where the Dirichlet condition is implemented by choosing  $Q = -1$  on  $\Gamma_1$  and  $u_{ex}(r, \theta) = J_{2/3}(\kappa r) \sin(2\theta/3)$ , where  $r = |x|$ . This exact solution  $u = u_{ex}$  has a singular gradient at the origin (of course  $u_{ex} \in H^1(\Omega)$ ).

In the first  $L$ -shaped domain example we compare the accuracy of plane wave basis and the Bessel bases. For the uniform mesh (Fig. 5(a)) the number of basis functions per element is chosen by trying to keep the error roughly constant.

However, in practice it is efficient to use a non-uniform mesh. For a non-uniform mesh we must vary  $p_k$  to control conditioning and choose the number of basis functions as in [16] by

$$p_k = \text{round}(\kappa_k h_k + C(\kappa_k h_k)^{\frac{1}{3}}), \quad (4.2)$$

where  $h_k$  is the length of the longest edge of the element,  $C$  is a constant ( $C = 5$  in our simulations below unless otherwise stated) and if  $p_k$  is even we set  $p_k = p_k - 1$ . We have not proved that (4.2) is optimal but we have found that it works rather well, for example, in reference [16], (formula (4.2) is motivated by the theory of fast multipole method [5]).

Because of the varying element size the errors in this section are computed from

$$\text{error}(\%) = \frac{\|u_{app} - u_e\|_{L^2}}{\|u_e\|_{L^2}} \times 100\%. \quad (4.3)$$

Results are shown in Table 2.

From Table 2 we see that using Bessel bases we obtain almost the same error as when using the same number of plane wave basis functions when the uniform mesh is used.

Table 2: On the uniform and lightly refined meshes for the  $L$ -shaped domain we show results for the plane wave basis, Bessel without scaling basis and scaled Bessel basis (terms in denominator  $L_k = h_{\max}^k$  (the maximum of an element  $\Omega_k$  edge)). The number of basis functions on element  $\Omega_k$  is denoted by  $p$ , the wavenumber is  $\kappa$ , the maximum of 1-norm condition number of elementwise block matrix  $\mathbf{D}$  is  $\max(\text{Dcond})$  and the error is computed from (4.3).

Basis	$\kappa$	Uniform mesh			Lightly refined mesh		
		$p$	error (%)	max (Dcond)	$p$	error (%)	max (Dcond)
PW	0.05	5	1.5173	1.3196e6	3	0.4999	11.2229
	0.5	5	1.0571	1.3132e4	3	0.4791	11.1942
	5	7	1.8760	4.7782e3	3...7	2.6257	2.3514e4
	50	25	2.8962	3.3511e5	7...27	2.1779	1.2786e8
Bessel	0.05	5	1.5173	1.0516e6	3	0.4971	8.6893
	0.5	5	1.0573	1.0723e4	3	0.4588	8.6974
	5	7	1.8527	4.2595e3	3...7	2.0908	2.1132e4
	50	25	2.8893	2.6502e5	7...27	2.1539	1.1437e8
scaled Bessel ( $h_{\max}^k$ )	0.05	5	1.5173	6.0353e3	3	0.4971	4.4679e5
	0.5	5	1.0573	61.6910	3	0.4588	4.4679e3
	5	7	1.8527	349.0382	3...7	2.0908	130.8977
	50	25	2.8893	2.4433e7	7...27	2.1539	1.2311e14

Moreover, for the uniform mesh case similar behavior of the maximum condition number of matrix  $\mathbf{D}$  can be noticed for the plane wave basis and Bessel basis without scaling as is to be expected following our previous simulation of propagating plane wave and evanescent wave. Results shown in Table 2 for the lightly refined non-uniform mesh demonstrate that we obtain similar accuracy levels for plane wave basis and Bessel basis which are consistent with uniform mesh results. For the non-uniform mesh the number of basis functions on each element is given by Eq. (4.2). Results show that the scaled Bessel basis may even increase the condition number although errors are similar for scaled and unscaled Bessel bases.

Next we use a slightly different approach to this problem applying the modified Bessel basis in which we take into account the singularity in the exact solution. The modified Bessel basis is defined by

$$\varphi_{k,\ell} = \begin{cases} J_{|\ell|}(\bar{\kappa}_k |\mathbf{x}_k - \mathbf{x}_{0,k}|) e^{i\ell\theta}, & \text{in } \Omega_k \text{ and if } \ell = -\frac{2}{3}, \\ J_{\ell}(\bar{\kappa}_k |\mathbf{x}_k - \mathbf{x}_{0,k}|) e^{i\ell\theta}, & \text{in } \Omega_k \text{ and if } \ell \neq -\frac{2}{3}, \\ 0, & \text{elsewhere,} \end{cases}$$

the order  $\ell$  of Bessel function in an element  $\Omega_k$  is

$$\ell = \begin{cases} s - \frac{p_k - 3}{2} - 1, & \text{when } s = 1, \dots, p_k - 2, \\ \frac{2}{3}, & \text{when } s = p_k - 1, \\ -\frac{2}{3}, & \text{when } s = p_k. \end{cases}$$

Table 3: Results for the uniform and lightly refined  $L$ -shaped domain using plane wave (PW), modified Bessel and PW+modified Bessel basis functions. The number of basis functions on element  $\Omega_k$  is denoted by  $p$ , wavenumber is  $\kappa$ , the maximum of 1-norm condition number of elementwise block matrix  $\mathbf{D}$  is  $\max(\text{Dcond})$  and error is calculated using (4.3).

Basis	$\kappa$	Uniform mesh			Lightly refined mesh		
		$p$	error (%)	max (Dcond)	$p$	error (%)	max (Dcond)
PW	0.05	5	1.5173	1.3196e6	3	0.4999	11.2229
	0.5	5	1.0571	1.3132e4	3	0.4791	11.1942
	5	7	1.8760	4.7782e3	3...7	2.6257	2.3514e4
	50	25	2.8962	3.3511e5	7...27	2.1779	1.2786e8
modified Bessel	0.05	5	1.0836	1.0511e6	3	2.3495	65.0767
	0.5	5	0.2504	1.0723e4	3	0.4688	14.3588
	5	7	0.0931	4.2595e3	3...7	1.2629	2.1132e4
	50	25	0.0208	2.6588e7	7...27	0.0336	1.1437e8
PW+modified Bessel	0.05	5	1.0827	1.3196e6	3	2.3529	65.0767
	0.5	5	0.2498	1.3132e4	3	0.4960	14.3588
	5	7	0.1194	4.7782e3	3...7	1.8532	2.3514e4
	50	25	0.0246	2.6588e7	7...27	0.0454	1.2786e8

The modified Bessel basis is used only in elements which share the vertex at the singular point. Moreover, we set the modified Bessel basis origin, i.e.,  $x_{0,k}$ , to the singular point  $x_{0,k} = (0,0)$ . The basis reflects the known singular behavior at that vertex.

Because of quadratures, it is not efficient to use the Bessel basis everywhere in the computational domain. Instead we use a regular plane wave basis and modified Bessel basis in the same mesh. We use the modified Bessel basis functions on elements that share a vertex at the singular point and elsewhere we use the plane wave basis. Results are shown in Table 3 using uniform mesh (Fig. 5(a)) and lightly refined mesh (Fig. 5(b)). For the uniform mesh the number of basis functions per element is chosen by trying to keep roughly constant the error level. In the case of non-uniform mesh the number of basis functions is computed from (4.2).

For the uniform mesh, Table 3 shows that the singularity at  $(0,0)$  adversely effects the accuracy using a plane wave basis particularly at high frequencies. In addition, we see that using the modified Bessel basis in the uniform mesh we can get more accurate results than using a pure plane wave basis. Moreover, if  $\kappa$  is high, the effect of the modified Bessel is better at improving the accuracy, and we see that it is possible to use the coupling of a plane wave basis and a modified Bessel basis. If  $\kappa = 0.05, \dots, 5$  the worst condition number comes from an element where the plane wave basis is used because it is the same for both plane wave basis case and plane wave+Bessel basis case. The lightly refined mesh (Fig. 5(b)) results are similar to the uniform mesh results. We emphasize that the number of basis functions were chosen differently in the uniform mesh case and for graded meshes. In the case of the lightly refined mesh the modified Bessel basis does not help the accuracy much if  $\kappa \neq 50$ .

Finally we consider the densest mesh (Fig. 5(c)) when the accuracy parameter  $C = 5$  and  $C = 8$  in Eq. (4.2). Results are shown in Table 4. As before the modified Bessel basis

Table 4: Results using the plane wave and plane wave+modified Bessel basis functions in a non-uniform mesh (the densest mesh right in Fig. 5). The number of basis functions on element  $\Omega_k$  is denoted by  $p$ , wavenumber is  $\kappa$ , the maximum of 1-norm condition number of elementwise block matrix  $\mathbf{D}$  is  $\max(\text{Dcond})$  and the error is calculated from (4.3).

Basis	$\kappa$	$p$	error (%)	max (Dcond)
PW ( $C=5$ )	0.05	3	0.1862	9.1622
	0.5	3	0.1917	9.1622
	5	3...5	1.2076	1.3343e3
	50	3...17	1.0350	5.0378e6
PW+ modified Bessel ( $C=5$ )	0.05	3	0.1875	2.2074e3
	0.5	3	0.1928	475.5730
	5	3...5	1.2125	1.3343e3
	50	3...17	1.0761	5.0378e6
PW ( $C=8$ )	0.05	3	0.1862	9.1622
	0.5	3	0.1917	9.1622
	5	3...7	0.0848	1.1854e6
	50	5...23	0.0933	2.4522e11
PW+modified Bessel ( $C=8$ )	0.05	3	0.1875	2.2074e3
	0.5	3	0.1928	475.5730
	5	3...7	0.0901	1.1854e6
	50	5...23	0.1370	2.4522e11

is only on elements near the singular point i.e., the modified Bessel basis is used on five elements that touch  $(0,0)$ .

Table 4 demonstrates that properly refining the grid near the singular point enhance the accuracy and that plane waves can approach the accuracy of the modified Bessel method, mitigating the pollution from the singularity. The modified Bessel basis does not help the accuracy and therefore plane wave basis and plane wave+modified Bessel basis results do not differ much. As we expect the  $C$  parameter affects on the accuracy. However, the condition number of matrix  $\mathbf{D}$  increases as the number of basis functions  $p_k$  increases.

## 5 Conclusions

In this paper we investigate the use of Bessel functions in the UWVF. Our first numerical example shows that Bessel bases work better than the plane wave basis for the propagating plane wave problem in a rectangular domain. However, the accuracy levels of plane wave basis and Bessel bases were almost the same for the evanescent wave problem. Results also show that using Bessel basis with scaling results in a lower condition numbers for the block matrix  $\mathbf{D}$  (if  $p > 3$ ). The effect of ill-conditioning was seen for the plane wave basis when the element size was small whereas the increasing condition number did not increase the error for the Bessel basis with or without scaling. On the other hand, in the evanescent wave problem the ill-conditioning did not affect the accuracy levels either for

the plane basis or for the Bessel bases. However, in the evanescent wave problem error levels were higher than in plane wave propagation model problem. If very high accuracy is needed, the Bessel bases are more robust. However, for an error of around 1% our results suggest to use the plane wave basis functions in the UWVF. Taking into account the cost of quadratures in the case of Bessel bases reinforces this view.

For the singular 2-D Helmholtz problem, the Bessel basis without scaling worked similarly to the plane wave basis. Our results clearly show the pollution effect of the singularity on the error particularly at higher  $\kappa$ . Two remedies are available. The first is to couple the plane wave basis and modified Bessel basis. Results show that the plane wave and modified Bessel basis improve the accuracy in the case of a uniform mesh. However, in the case of a non-uniform mesh, when the elements were small compared to wavelength the modified Bessel basis did not work well and at low wavenumbers the errors increased. The second approach, also applicable in three dimensions, is to use plane waves on a suitably refined mesh.

## Acknowledgments

Authors would like to thank Vilho, Yrjö and Kalle Väisälä Fund, Saastamoinen's Foundation, Finnish Cultural Foundation: North Savo Regional Fund, Emil Aaltonen's Foundation, Finnish Centre of Excellence in Inverse Problems Research and the US AFOSR for their support.

## References

- [1] D. Arnold, F. Brezzi, B. Cockburn and L. Marini, Unified analysis of discontinuous Galerkin methods for elliptic problems, *SIAM J. Numer. Anal.*, 42(6) (2002), 1749–1779.
- [2] Z. Badics and Y. Matsumoto, Trefftz discontinuous Galerkin methods for time-harmonic electromagnetic and ultrasound transmission problems, *Int. J. Appl. Electromagn. Mech.*, 28(1-2) (2008), 17–24.
- [3] A. H. Barnett and T. Betcke, An exponentially convergent nonpolynomial finite element method for time-harmonic scattering from polygons, submitted.
- [4] A. Buffa and P. Monk, Error estimates for the ultra weak variational formulation of the Helmholtz equation, *ESAIM: M2AN Math. Model. Numer. Anal.*, 42(6) (2008), 925–940.
- [5] Q. Carayol and F. Collino, Error estimates in the fast multipole method for scattering problems, part 1: truncation of the Jacobi-Anger series, *ESAIM: Math. Model. Numer. Anal.*, 38(2) (2004), 371–394.
- [6] O. Cessenat, Application d'une Nouvelle Formulation Variationnelle aux Équations D'ondes Harmoniques, Problèmes de Helmholtz 2D et de Maxwell 3D, PhD thesis, Université Paris IX Dauphine, 1996.
- [7] O. Cessenat and B. Després, Application of an ultra weak variational formulation of elliptic PDEs to the two-dimensional Helmholtz problem, *SIAM J. Numer. Anal.*, 35(1) (1998), 255–299.

- [8] O. Cessenat and B. Després, Using plane waves as base functions for solving time harmonic equations with the ultra weak variational formulation, *J. Comput. Acoust.*, 11(2) (2003), 227–238.
- [9] C. Farhat, I. Harari and L. P. Franca, A discontinuous enrichment method, *Comput. Methods Appl. Mech. Eng.*, 190(48) (2001), 6455–6479.
- [10] C. Farhat, I. Harari and U. Hetmaniuk, A discontinuous Galerkin method with Lagrange multipliers for the solution of Helmholtz problems in the mid-frequency regime, *Comput. Methods Appl. Mech. Eng.*, 192(11-12) (2003), 1389–1429.
- [11] G. Gabard, Discontinuous Galerkin methods with plane waves for time-harmonic problems, *J. Comput. Phys.*, 225(2) (2007), 1961–1984.
- [12] P. Gamallo and R. J. Astley, Comparison of two Trefftz-type methods: the ultraweak variational formulation and the least-squares method, for solving shortwave 2-D Helmholtz problems, *Int. J. Numer. Methods Eng.*, 71(4) (2007), 406–432.
- [13] G. Gabard, P. Gamallo and T. Huttunen, A comparison of Trefftz, discontinuous Galerkin, ultra-weak and least-square methods for wave problems, submitted.
- [14] C. Gittelsohn, R. Hiptmair and I. Perugia, Plane wave discontinuous Galerkin methods: analysis of the  $h$ -version, *ESAIM: M2AN Math. Model. Numer. Anal.*, 43(2) (2009), 297–331.
- [15] R. Hiptmair, A. Moiola and I. Perugia, Plane wave discontinuous Galerkin methods for the 2D Helmholtz equation: analysis of the  $p$ -version, *SAM-ETH Zurich Report 2009-20*, 2009-20, 1–20.
- [16] T. Huttunen, P. Gamallo and R. J. Astley, Comparison of two wave element methods for the Helmholtz problem, *Commun. Numer. Methods Eng.*, 25(1) (2009), 35–52.
- [17] T. Huttunen, M. Malinen, J. P. Kaipio, P. J. White and K. Hynynen, A full-wave Helmholtz model for continuous-wave ultrasound transmission, *IEEE T. Ultrason. Ferr.*, 52(3) (2005), 397–409.
- [18] T. Huttunen, M. Malinen and P. Monk, Solving Maxwell's equations using the ultra weak variational formulation, *J. Comput. Phys.*, 223(2) (2007), 731–758.
- [19] T. Huttunen, P. Monk, F. Collino and J. P. Kaipio, The ultra weak variational formulation for elastic wave problems, *SIAM J. Sci. Comput.*, 25(5) (2004), 1717–1742.
- [20] T. Huttunen, P. Monk and J. P. Kaipio, Computational aspects of the ultra-weak variational formulation, *J. Comput. Phys.*, 182(1) (2002), 27–46.
- [21] T. Huttunen, E. T. Seppälä, O. Kirkeby, A. Kärkkäinen and L. Kärkkäinen, Simulation of the transfer function for a head-and-torso model over the entire audible frequency range, *J. Comput. Acoust.*, 15(4) (2007), 429–448.
- [22] M. Loeser and B. Witzigmann, The ultra weak variational formulation applied to radiation problems with macroscopic sources in inhomogeneous domains, *IEEE J. Sel. Top. Quant.*, 15(4) (2009), 1144–1155.
- [23] J. M. Melenk and Babuška, The partition of unity finite element method: basic theory and applications, *Comput. Methods Appl. Mech. Eng.*, 139(1-4) (1996), 289–314.
- [24] P. Monk and D. Q. Wang, A least-squares method for the Helmholtz equation, *Comput. Methods Appl. Mech. Eng.*, 175(1-2) (1999), 121–136.
- [25] P. Monk, J. Schöberl and A. Sinwel, Hybridizing Raviart-Thomas elements for the Helmholtz equation, submitted *RICAM REPORT 2008-22*.
- [26] E. Perrey-Debain, Plane wave decomposition in the unit disc: convergence estimates and computational aspects, *J. Comput. Appl. Math.*, 193 (2006), 140–156.